

# Single Image Internal Distribution Measurement Using Non-Local Variational Autoencoder

Yeahia Sarker, *Student Member, IEEE*, Abdullah-Al-Zubaer Imran, Md Hafiz Ahamed, *Graduated Member, IEEE*, Ripon K. Chakraborty, Michael J. Ryan, *Senior Member, IEEE*, Sajal K. Das, *Member, IEEE*

**Abstract**—(This is a preprint). Deep learning-based super-resolution methods have shown great promise, especially for single image super-resolution (SISR) tasks. Despite the performance gain, these methods are limited due to their reliance on copious data for model training. In addition, supervised SISR solutions rely on local neighbourhood information focusing only on the feature learning processes for the reconstruction of low-dimensional images. Moreover, they fail to capitalize on global context due to their constrained receptive field. To combat these challenges, this paper proposes a novel image-specific solution, namely non-local variational autoencoder (NLVAE), to reconstruct a high-resolution (HR) image from a single low-resolution (LR) image without the need for any prior training. To harvest maximum details for various receptive regions and high-quality synthetic images, NLVAE is introduced as a self-supervised strategy that reconstructs high-resolution images using disentangled information from the non-local neighbourhood. Experimental results from seven benchmark datasets demonstrate the effectiveness of the NLVAE model. Moreover, our proposed model outperforms a number of baseline and state-of-the-art methods as confirmed through extensive qualitative and quantitative evaluations.

**Index Terms**—self-supervised learning, image super-resolution, variational autoencoder, zero-shot learning.

## I. INTRODUCTION

Image super-resolution (SR) refers to the task of recovering a latent high-resolution (HR) image from a corresponding low-resolution (LR) image. This has been one of the most widely explored inverse problems in computer vision [1], [2]. A LR image  $I_x$  is assumed to be modeled as the output of the following degradation:

$$I_x = \mathbf{D}(I_y; \lambda). \quad (1)$$

where  $\mathbf{D}$  defines a degradation mapping function,  $I_y$  is the corresponding HR image, and  $\lambda$  denotes the degradation parameter. The higher the degradation, the harder becomes

Yeahia Sarker is with the Department of Mechatronics Engineering, Rajshahi University of Engineering & Technology, Rajshahi 6204, Bangladesh. Email : yeahia.ruet@gmail.com

Abdullah-Al-Zubaer Imran is with Stanford University, Stanford, CA 94305, USA Email: aimran@stanford.edu

Md Hafiz Ahamed is with the Department of Mechatronics Engineering, Rajshahi University of Engineering & Technology, Rajshahi 6204, Bangladesh. Email : hafiz@mte.ruet.ac.bd

Ripon K. Chakraborty is with the School of Engineering and IT, University of New South Wales, Canberra 7916, Australia. Email : r.chakraborty@unsw.edu.au

Michael J. Ryan is with the Capability Systems Centre, University of New South Wales, Canberra 7916, Australia. Email : m.ryan@unsw.edu.au

Sajal K. Das is with the Department of Mechatronics Engineering, Rajshahi University of Engineering & Technology, Rajshahi 6204, Bangladesh. Email : das.k.sajal@gmail.com

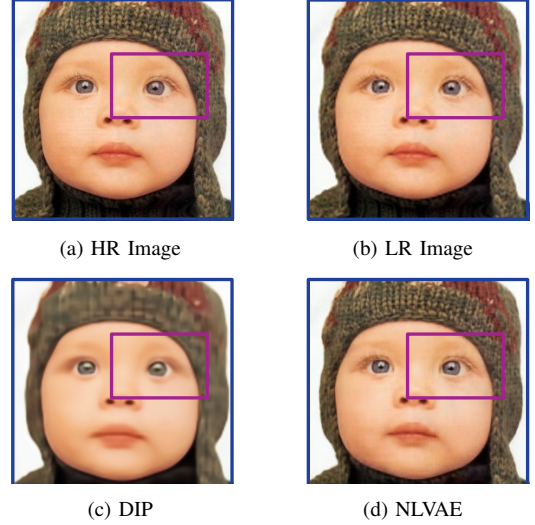


Fig. 1: Visual Comparison of Deep Image Prior (DIP) (untrained) & NLVAE (untrained)

the task to reconstruct the HR image [3]. The image super-resolution problem is also explored in the fields of remote sensing [4], surveillance imaging [5], and medical imaging [6]. While a number of approaches have been attempted to solve this problem, it remains ill-posed particularly since any specific LR image may correspond to croppings from multiple HR counterparts. Three types of solutions are usually provided to solve the SR problem; interpolation-based [7], learning-based [8], [9], [10] and reconstruction-based [11], [12], [13]. Learning-based SR methods learn the non-linear mapping between HR and LR image using probabilistic generative models, random forest, linear or non-linear models, neighbor embedding [14] and sparse regression [15]. Interpolation-based methods utilize the adjacent pixels to calculate the interpolated pixels by using an interpolation kernel. Several types of existing interpolation-based models have been used to tackle the SR problem such as bicubic[16], edge-directed estimation [17], and auto-regressive models [18]. Interpolation-based methods are very computationally efficient and relatively simple than other architectures. However, these methods suffer from low accuracy compared to other methods because of poor representation learning capacity [19].

Learning-based solutions are widely used in the SR task. They can primarily be categorized into three types: Code-based[20], [21], [9], CNN-based [22], [23] and regression-based [24]. In the past, learning-based solutions have shown

great success for image super-resolution due to a robust feature learning capability [25], [26]. The regression-based solutions are much faster than any other methods but, compared to other learning-based methods, produce blurry images and low peak-signal-noise ratio, due to poor representation learning [15], [10]. Learning-based solutions generally measure the similarity between LR & HR images. A number of methods have been proposed to solve this problem but among them, CNN-based methods have superior performance because of their robust representation learning capabilities [27]. As a learning-based method, a hierarchical pyramid structure was developed using residual layers for image super-resolution [28].

Zhang *et al.* [29] introduced residual dense block in order to learn hierarchical feature maps, utilizing a bottleneck layer at the end of the residual dense layer. The local connection in the same block represents short-term memory and skip connections define long-term memory for representation learning. Lim *et al.* [30] proposed Enhanced Deep Super-Resolution (EDSR) with a huge improvement in performance utilizing the residual structure. Despite the excellent performance, these methods utilize residual structure that is computationally resourceful. In [31], a combination of channel-wise attention and spatial attention block was developed for single image super-resolution (SISR). Both of these blocks were again combined with residual creating robust SR methods. This method captures sufficient representations from feature space and suppresses irrelevant information. As this approach combines two kinds of attention block with a stacked neural network, it consumes large amounts of memory and slows down the training process.

In [32], an autoencoder-based SISR method has been introduced with symmetric skip connections. Similarly, Tai *et al.* [33] featured a deep recursive residual network (DRRN) utilizing memory block with residual representation learning. These solutions provide better results with the help of large scale architecture. Park *et al.* [34] introduced a high dynamic range for super-resolution task that is very lightweight and easy to implement but decomposing the image causes loss of important information which results in low peak-signal noise ratio (PSNR) values.

Many upsampling strategies have been observed in the literature. Efficient sub-pixel CNN (ESPCN) uses sub-pixel convolution for upsampling [35] that stores channel information for extra points then reorganizes those points for HR reconstruction. Fast super-resolution CNN (FSRCNN) utilizes deconvolution operation to upsample [36]. Hua *et al.* used a deconvolution operation for the upsampling process, featuring the arbitrary interpolation operator and subsequent convolution operator [37]. It is to be noted that the deconvolution operation has two disadvantages: deconvolution is used at the end of the network, and the downsampling kernel is not known. Unknown input estimation consequently results in poor performance. To avoid these issues, we utilize linear upsampling of LR images so that we only focus on reconstruction quality rather than upsampling kernels.

From a theoretical perspective, it can be deduced that the deeper neural architecture provides better result than shallow

architecture [38]. Keeping this in mind, Kim *et al.* [22] first proposed a very deep architecture for SISR task. With 20 layers, VGGNet uses 3x kernels for all layers. Additionally, this method uses a high learning rate for faster convergence and utilizes gradient clipping to alleviate the gradient explosion problem. To learning short-term memory information, skip connections have been used in many tasks. Another work introduced recursive topology with parameter reduction using recursive convolution kernel [33]. However, these settings are risky as self-supervised settings because a faster learning rate will provide shallow feature learning process, thus resulting in poor performance.

Several reconstruction-based SISR methods have been introduced to solve the SISR problem, utilizing a shallow feature learning process [39], [40]. KernelGAN [41], consisting of a deep linear generator and a discriminator, supports blind SISR. A deep linear generator removes non-linear activation functions, but the overall loss function is not convex. The discriminator uses fully convolutional layers with no strides and pooling. Even though the overall structure means that the model converges faster, it is still difficult to obtain the global minimum. Our method utilizes the non-linear activation function in both encoder and decoder, making network learn more intuitive information than KernelGAN. Shaham *et al.* [42] proposed a multidisciplinary generative model capable of performing multiple computer vision tasks. To our knowledge, this work was the first attempt to use an unconditional generative model for the ZSSR task. It utilizes an adversarial network as a reconstruction-based method learning only abstract features from image patches. Due to the complexity of training an adversarial network, GAN models often suffer from convergence failure and mode collapse. Moreover, training adversarial training takes longer than discriminative models.

To alleviate these problems, we have devised an image-specific architecture, called probabilistic non-local variational neural autoencoder (NLVAE), which can generate high-quality images with a robust pixel learning capability. Our generative solution is specifically designed for ZSSR, storing more disentangled and intuitive features and learning from low-dimensional space.

Our specific contributions can be summarized as follows:

- An unconventional internal method has been introduced for the ZSSR task where only one LR image and its corresponding HR image are required for the training process. The proposed method is completely unsupervised and does not require any prior training. It establishes a new state-of-the-art (SOTA) which outperforms currently available methods.
- The proposed light-weight non-local feature extraction module harvests maximum representations from different receptive regions boosting the super-resolution performance.
- The proposed loss function aids to reconstruct high quality images by controlling the Lagrange multiplier and marginal value.

The rest of the paper is organized as follows. Section II shows some works related to our proposed network structure. Section III describes the working principle of our method.

In section IV, we provide quantitative and qualitative results using our model. Section V provides some ablation studies demonstrating the robustness of our network and section VI discusses the limitation of our strategy along with similarities and dissimilarities with other methods. Section VII provides concluding remarks.

## II. RELATED WORK

**Generative Models.** Generative models have been proven to reconstruct finer texture details and are able to generate more photo-realistic images than CNN-based methods. While shallow CNN-based SR methods provide detailed low-frequency information, GAN-based methods as generative models can discover high-frequency information. Super-Resolution GAN (SRGAN) [43] makes use of perceptual loss as well as residual dense network generating high-resolution images. Wang *et al.* [44] proposed residual-in-residual without batch normalization which produced HR images through adversarial training. Majdabad *et al.* [45] attached a capsule network as a complex network with GAN for face super-resolution. In [46], a conditional GAN has been introduced using ground-truth as a conditional variable for the discriminator. Similar to conditional GAN, conditional autoregressive generative models utilize maximum likelihood estimation depending on conditions. Based on these conditions, the generated HR images are reconstructed based on previous learned pixels [47], [48]. However, these generative models suffer from mode collapse and convergence failure problems [49]. Moreover, these methods are computationally expensive and integration with self-supervised training is quite difficult to implement as GAN-based methods require more image data for training than learning-based methods [50], [44].

**Non-Local Networks.** Non-local networks usually comprise an attention module with non-local blocks. Wang *et al.* [51] proposed a deformable non-local attention module for video super-resolution. In [52], a non-local recurrent model was introduced for SISR task, which can learn deep feature correlation among neighbourhood locations of patches. Zhang *et al.* [29] featured residual network with non-local attention units for image super-resolution. Another work presents a cross-scale non-local attention module for learning intrinsic feature correlations of images [53].

**Zero-Shot Super-Resolution Methods.** Shocher *et al.* [54] introduced the term "ZSSR," presenting a shallow CNN model to learn the probability distribution of the LR and HR images. The major disadvantage of this network is that it extracts local features utilizing a simple CNN architecture and a shallow CNN model, which also results in poor performance. Another internal method proposed in [55], introducing Deep Image Prior (DIP) to build a bridge between a CNN and convolutional sparse coding. The solution takes the neural network as the output of the reconstruction and random input signals. This is the first approach which creates a bridge between a code-based method and a learning-based method for ZSSR. Untrained DIP basically focuses on the smaller receptive fields for intuitive neural representation, but loses more context as feature extraction is limited to the smaller regions. Fig. 1 depicts that DIP

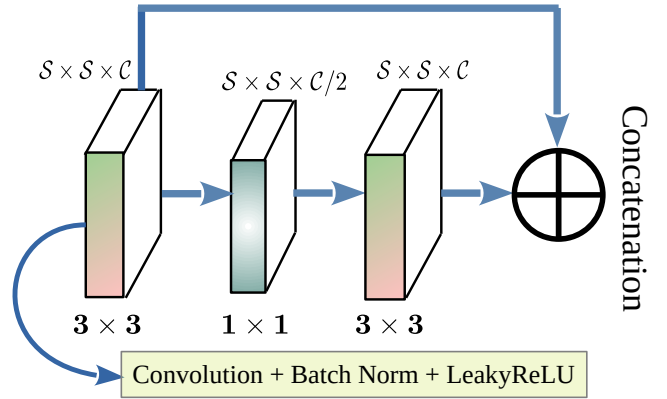


Fig. 2: Overview of non-local block used in our NLVAE network. The non-local block is composed of  $3 \times$  kernels and  $1 \times$  kernels. The initial convolution kernel is concatenated with the last feature transform to learn relative positional features.  $S \times S$  defines the spatial size of the feature and the channel information is denoted as  $C$ .

method shows very weak structural information compared to NLVAE. Due to a weak feature extraction process, this method suffer from low accuracy in terms of performance metrics [56].

## III. NETWORK STRUCTURE

In this section, we demonstrate the structure of our proposed non-local block in the neural encoder and decoder. We also show the measurement of posterior distribution and loss function and we provide a full analysis of how the Lagrange multiplier controls the reconstruction quality of generated image.

### A. Non-Local Encoder-decoder

As shown in Fig. 3, our proposed NLVAE model consists of an encoder and a decoder consisting of non-local convolution blocks. Fig. 2 depicts the overview of non-local blocks. The non-local block utilized in NLVAE can exploit spatial correlation between neighbourhood and locations. To design a computationally effective spectral correlation module, we have overlooked residual structure. Each non-local block is composed of convolution blocks and each convolution block comprises of 2D convolution, point-wise convolution and batch normalization [57] followed by Leaky-ReLU activation function. The encoder encodes the input image  $x$  into the latent representation  $z$  ( $z = \psi(x)$ ) and the decoder reconstructs the representation back to its approximate original data. We assume that the low-resolution image is an input vector denoted by  $x$  and  $z$  denotes the latent representation. The latent variables are controlled by a Gaussian distribution along with a diagonal covariance matrix. The latent space dimension is denoted by  $J$ . The output of the non-local convolutional encoder comprises a mean  $\mu$  and a log of variances  $\log(\sigma)$ . Through the reparameterization trick, a noise vector ( $\epsilon$ ) is obtained from the latent space [58]. The goal of the NLVAE model is the ability to produce a high-resolution reconstructed image from the low-resolution image, exploiting the relationship between the input vector and prior distribution  $p(z)$ .

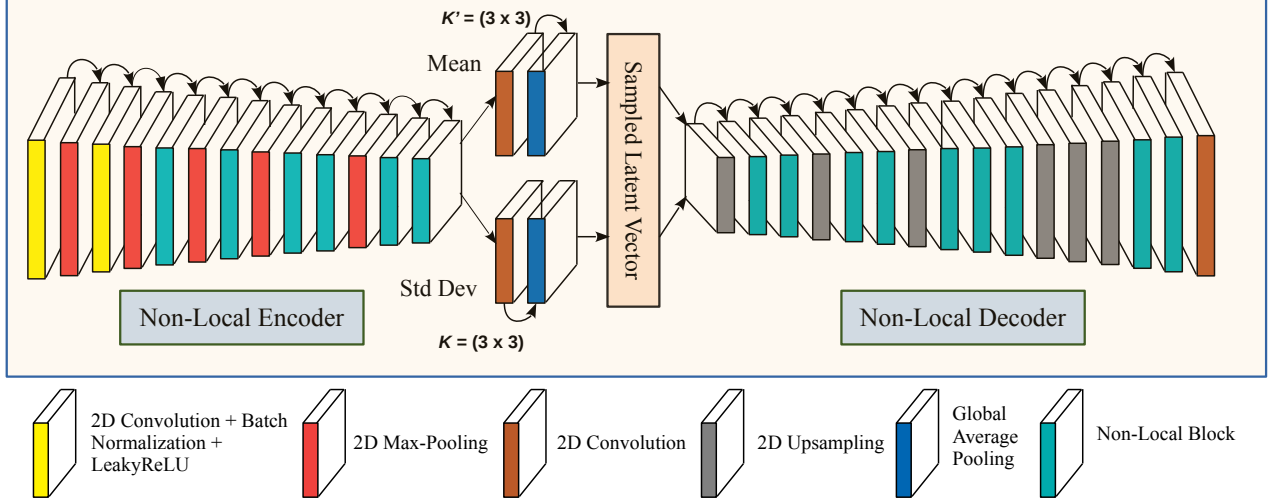


Fig. 3: Network structure of the proposed non-local variational autoencoder (NLVAE) model. Probabilistic encoder-decoder are composed of non-local units and various convolution and upsampling layers. The reconstruction quality is controlled by the operator  $\beta$ . Global avg pooling are used to calculate the mean and variance leveraging global structural details during the reconstruction process.

---

**Algorithm 1: Training NLVAE model**


---

**Input :** Initialize network parameters  
**while** not converged **do**  
 $\mathbf{X} =$  pseudo labels of single  $L_r$  image  
 $Z_p \leftarrow$  Distribution from prior  $\mathbf{N}(0, I)$   
 $Z_r \leftarrow \text{Non-LocalEncoder}(\mathbf{X})$   
 $X_r \leftarrow \text{Non-LocalDecoder}(Z)$   
 $X_p \leftarrow \text{Non-LocalDecoder}(Z_p)$   
 $L_{KL} \leftarrow L_{KL}(X_r, X_p)$   
 $\phi_E \leftarrow \phi_E - \eta \nabla_{\phi_E}(L_R + \beta L_{AE})$   
 (Updating Adam for  $\phi_E$ )  
**end**

---

### B. Posterior Distribution

We denote the low-resolution input data distribution as  $x$   $p_d(x)$  and the high-resolution reconstructed data distribution as  $\bar{x}$   $p(x)$ . The encoded and decoded data distributions are represented as  $q_\phi(z|x)$  and  $p_\theta(z|x)$  respectively, where  $\phi$  and  $\theta$  are the variables of the encoder and decoder networks. The  $q(x)$  tries to approximate the output prior  $p(z)$ . Centered isotropic multivariate Gaussian  $\mathbf{N}(0, I)$  was chosen as the prior  $p(z)$  over the latent variables [59]. The inference model is designed to output two individual variables  $\mu$  and  $\sigma$ , and thus the posterior  $q_\phi(z|x) = \mathbf{N}(z; \mu, \sigma_2)$ . With this setting, to get the desired prior distribution, the non-local convolutional encoder and decoder are trained to optimize the reconstruction error (that is, the mean squared error). The loss function tries to approximate between each patch of LR and HR over a fake minibatch  $x_n$  where  $n$  is the size of the fake minibatch. The total number of data points is denoted as  $N$ .

The input of the decoder is sampled from  $\mathbf{N}(z; \mu, \sigma_2)$  using a reparameterization trick  $z = \mu + \sigma \odot \epsilon$  where  $\epsilon = \mathbf{N}(0, I)$ . The aggregated posterior distribution is defined as  $z = q(z)$ :

$$q(\mathbf{z}) = \int_{\mathbf{x}} q_\phi(\mathbf{z}|\mathbf{x}) p_d(\mathbf{x}) d\mathbf{x}. \quad (2)$$

### C. Loss Function

It is useful to prepare the low-resolution input image by clustering in latent space, eradicating the noise  $L_R$  loss is summed over the data points and the average of the fake minibatch is calculated. Thus, it provides more weight to the reconstruction error helping reduce potential model collapse.

$$L_R(\phi, \theta; x_M, \epsilon) = \frac{1}{M} \sum_{i=1}^M \sum_{j=1}^N (x_{i,j} - \hat{x}_{i,j})^2. \quad (3)$$

To obtain the desired prior distribution,  $KL$  divergence is utilized on the encoded variable to measure the probability distance of LR and HR images.  $KL$  divergence is calculated over the fake minibatch as

$$L_{KL}(\phi; x_M) = \frac{1}{M} \sum_{i=1}^M \sum_{j=1}^J (1 + \log(\sigma_{i,j}^2) - \mu_{i,j}^2 - \sigma_{i,j}^2). \quad (4)$$

Therefore, the total loss is calculated as

$$L_{BETA}(\phi, \theta; x_M, \epsilon) = L_R + \beta L_{KL} + \alpha \quad (5)$$

where  $\beta$  denotes the Lagrangian multiplier and  $\alpha$  denotes the marginal value. As the negation of  $L_{BETA}$  is the lower bound of the Lagrangian, minimization of the loss is equivalent to maximization of the Lagrangian, which is useful for our initial optimization problem. The  $\alpha$  controls the quality of image reconstruction as an aid to the objective function. For  $\beta = 1$ , the working principle is the same as traditional VAE. When  $\beta > 1$ , it applies a stronger constraint on the latent bottleneck and limits the representation capacity of  $z$  [60]. Maintaining the disentanglement is the most effective representation for some of the conditionally independent generative factors [61].

### D. Lagrangian multiplier variation for different upscaling

The addition of  $\beta$  in VAE provides more disentangled information and sharp gradients compared to traditional VAE [62].

A higher value of  $\beta$  provides more efficient encoded latent vectors and further encourages disentanglement. However, too large  $\beta$  may lead to poorer reconstruction quality as it creates a trade-off with the extent of disentanglement. The reconstruction loss ensures the network captures useful information while forming the latent distribution. An increase in the number of latent variables reduces image quality, thus through empirical evaluation, we selected a different Lagrangian multiplier for different upscaling. For our experimental settings, we have selected 150, 200, and 300 for  $3 \times$ ,  $4 \times$ , and  $8 \times$  upscaling factor respectively.

### E. Computational Efficiency of Non-local Block

In this subsection, the computational efficiency of the non-local block is briefly explained. The point-wise convolution is the core of non-local block for calibrating spatial information. It also serves as the channel reduction technique in this network. The weights of the point-wise convolution can be calculated as:

$$W_{PC} = K \times K \times N \times P. \quad (6)$$

For this operation,  $K = 1$ . Then Equation 6 becomes:

$$W_{PC} = N \times P. \quad (7)$$

And the corresponding number of operations is therefore:

$$\begin{aligned} O_{PC} &= M \times M \times K \times K \times N \times P \\ &= M \times M \times N \times P. \end{aligned} \quad (8)$$

For the standard convolution operation, the number of weights will be:

$$W_{SC} = K \times K \times N \times P. \quad (9)$$

And the corresponding number of operation is:

$$O_{SC} = M \times M \times K \times K \times N \times P. \quad (10)$$

Now, the reduction factors of weights and operations can be defined as:

$$F_W = \frac{W_{PC}}{W_{SC}}. \quad (11)$$

$$F_O = \frac{O_{PC}}{O_{SC}}. \quad (12)$$

From the reduction factors of weights and operation, we can observe the reduction in computational cost due to the use of point-wise convolutions.

For the standard convolution operation, the number of weights will be

$$W_{SC} = K \times K \times N \times P. \quad (13)$$

And the corresponding number of operation is,

$$O_{SC} = M \times M \times K \times K \times N \times P. \quad (14)$$

Now, the reduction factors of weights and operations can be defined as

$$F_W = \frac{W_{PC}}{W_{SC}}. \quad (15)$$

$$F_O = \frac{O_{PC}}{O_{SC}}. \quad (16)$$

From the reduction factors of weights and operation, we can observe the reduction in computational cost due to the use of point-wise convolutions.

## IV. EXPERIMENTAL EVALUATIONS

### A. Datasets

We have evaluated our proposed NLVAE model against seven different datasets—Set5 [66], Set14 [67], BSD100 [68], Manga109 [69], Urban100 [70], General100 [36], and T19 [71]. In the qualitative analysis, we have used the General100, Set14, Set5, and T91 datasets, while the quantitative analyses are performed using the Set5, Set14, BSD100, Urban100, and Manga109 datasets. We have compared our model against a number of baseline and SOTA models, reporting PSNR and SSIM metrics.

### B. Implementation Details & Training Settings

We make use of the TensorFlow framework with Python for all the experiments. The experiments are implemented on a Nvidia GeForce GTX Titan X and Intel Xeon CPU at 2.40 GHz machine. All the images are resized to  $256 \times 256$ . The Adam optimizer [72] is utilized with  $\beta_1 = 0.9$ ,  $\beta_2 = 0.999$ , and  $\sigma = 10^{-8}$ . Pseudo labels are created for training purposes as there exists only one single image. The model is trained till 2000 epochs. We use the  $L_2$  loss function for our solution. For our settings, the hyperparameters are selected empirically. We perform the experiments for three different scaling factors— $3 \times$ ,  $4 \times$ , and  $8 \times$ . The value of  $\beta$  is set to 500 for all the experiments.

As the proposed method utilizes self-training strategy, it takes both  $L_R$  and  $H_R$  single image as input for training pipeline. Then, it tries to learn the relationship leveraging non-local attention blocks. Finally, the self-training model tries to generate a single  $H_R$  image from the pre-trained weights. It is to be noted that the performance metric calculation is the mean of all single generated images for each datasets.

### C. Results

1) *Quantitative*: Table I reports the quantitative results for ( $\times 3$ ), ( $\times 4$ ), ( $\times 8$ ) SR methods. Both learning-based (Bicubic, A+, Super-Resolution CNN (SRCNN), Fast SRCNN (FSRCNN), Very Deep Super-Resolution (VDSR), Laplacian Pyramid Super-Resolution Network (LapSRN), Memory Network (MemNet) and reconstruction-based methods (SRGAN, ESRGAN) have been compared against the proposed framework. It is worth mentioning that deeper architectures perform better over the shallower networks. We also note that larger scaling factors affect the performance of the existing external methods. Among learning-based methods, MemNet demonstrates good performance over large scaling factors because of its large architecture, but its performance drops when the scaling factor is relatively small. The reconstruction-based strategies have higher structural similarity than other methods. Most importantly, our proposed NLVAE model outperforms

TABLE I: Benchmark results for SISR methods. Best results are in bold. All the methods are trained on DIV2K datasets.

Scale	Method	Set5		Set14		BSDS100		Urban100		Manga109	
		PSNR	SSIM	PSNR	SSIM	PSNR	SSIM	PSNR	SSIM	PSNR	SSIM
$\times 4$	Bicubic	30.40	0.8684	27.55	0.7743	27.19	0.7388	24.45	0.7358	26.95	0.8558
	A+ [63]	32.51	0.9080	29.10	0.8202	28.21	0.7829	25.86	0.7891	29.90	0.9101
	SRCNN [64]	32.75	0.9090	29.30	0.8215	28.28	0.7832	25.87	0.7888	30.56	0.9124
	FSRCNN [36]	33.17	0.9141	29.39	0.824	28.59	0.7940	26.43	0.8075	31.05	0.9189
	VDSR [22]	33.67	0.9212	29.78	0.8318	28.83	0.7982	27.14	0.8280	32.07	0.9337
	LapSRN [28]	33.82	0.9227	29.84	0.8322	28.82	0.7982	27.07	0.8270	32.21	0.9342
	MemNet [65]	34.09	0.9248	30.00	0.8350	28.95	0.8001	27.53	0.8270	32.58	0.9382
	SRGAN [43]	33.73	0.9102	29.58	0.8215	28.62	0.7790	26.04	0.8168	31.56	0.9187
	NLVAE (Proposed)	<b>34.10</b>	<b>0.9270</b>	<b>30.81</b>	<b>0.8398</b>	<b>29.05</b>	<b>0.7805</b>	<b>28.07</b>	<b>0.8402</b>	<b>33.19</b>	<b>0.9437</b>
$\times 8$	Bicubic	28.43	0.8109	26.00	0.7026	25.95	0.6698	23.13	0.6598	24.89	0.7865
	A+ [63]	30.25	0.8601	27.21	0.7503	26.65	0.7103	24.19	0.7198	27.08	0.8519
	SRCNN [64]	30.48	0.8628	27.50	0.7513	26.90	0.7114	24.52	0.7221	27.60	0.8583
	FSRCNN [36]	30.72	0.8658	27.60	0.7538	26.95	0.7138	24.62	0.7280	27.86	0.8602
	VDSR [22]	31.35	0.8838	28.02	0.7682	27.29	0.7165	25.18	0.7530	28.87	0.8862
	LapSRN [28]	31.54	0.8860	28.16	0.7724	27.32	0.7161	25.21	0.7558	29.09	0.8890
	MemNet [65]	31.76	0.8893	28.26	0.7726	27.42	0.7280	25.50	0.7628	29.64	0.8938
	SRGAN [43]	29.37	0.8471	26.01	0.7396	25.13	0.6645	24.35	0.7331	28.39	0.8603
	ESRGAN [44]	30.47	0.8512	26.28	0.6987	25.32	0.6519	24.36	0.7337	28.44	0.8609
NLVAE (Proposed)	<b>31.96</b>	<b>0.8903</b>	<b>28.67</b>	<b>0.7776</b>	<b>27.86</b>	<b>0.7367</b>	<b>25.88</b>	<b>0.7751</b>	<b>30.11</b>	<b>0.8945</b>	
$\times 16$	Bicubic	24.42	0.6580	23.10	0.5660	23.65	0.5483	20.74	0.5160	21.55	0.6509
	A+ [63]	25.21	0.6875	23.48	0.5889	23.97	0.5605	21.02	0.5403	22.11	0.6813
	SRCNN [64]	25.33	0.6900	23.76	0.5910	24.13	0.5659	21.29	0.5438	22.40	0.6846
	FSRCNN [36]	20.13	0.5520	19.75	0.4820	24.21	0.5672	21.32	0.5379	22.39	0.6730
	VDSR [22]	25.95	0.7242	24.26	0.6140	24.37	0.5767	21.65	0.5704	23.16	0.7230
	LapSRN [28]	26.14	0.7384	24.35	0.6200	24.53	0.5865	21.81	0.5805	23.39	0.7533
	MemNet [65]	26.16	0.7414	24.38	0.6199	24.59	0.5843	21.88	0.5824	23.56	0.7386
	SRGAN [43]	25.88	0.7069	24.02	0.6015	24.41	0.5786	21.68	0.5614	24.61	0.7864
	ESRGAN [44]	26.30	0.7551	24.07	0.6011	24.64	0.5850	22.57	0.6279	24.75	0.7872
NLVAE (Proposed)	<b>27.23</b>	<b>0.7860</b>	<b>25.32</b>	<b>0.6469</b>	<b>25.31</b>	<b>0.5983</b>	<b>22.97</b>	<b>0.6353</b>	<b>25.12</b>	<b>0.8013</b>	

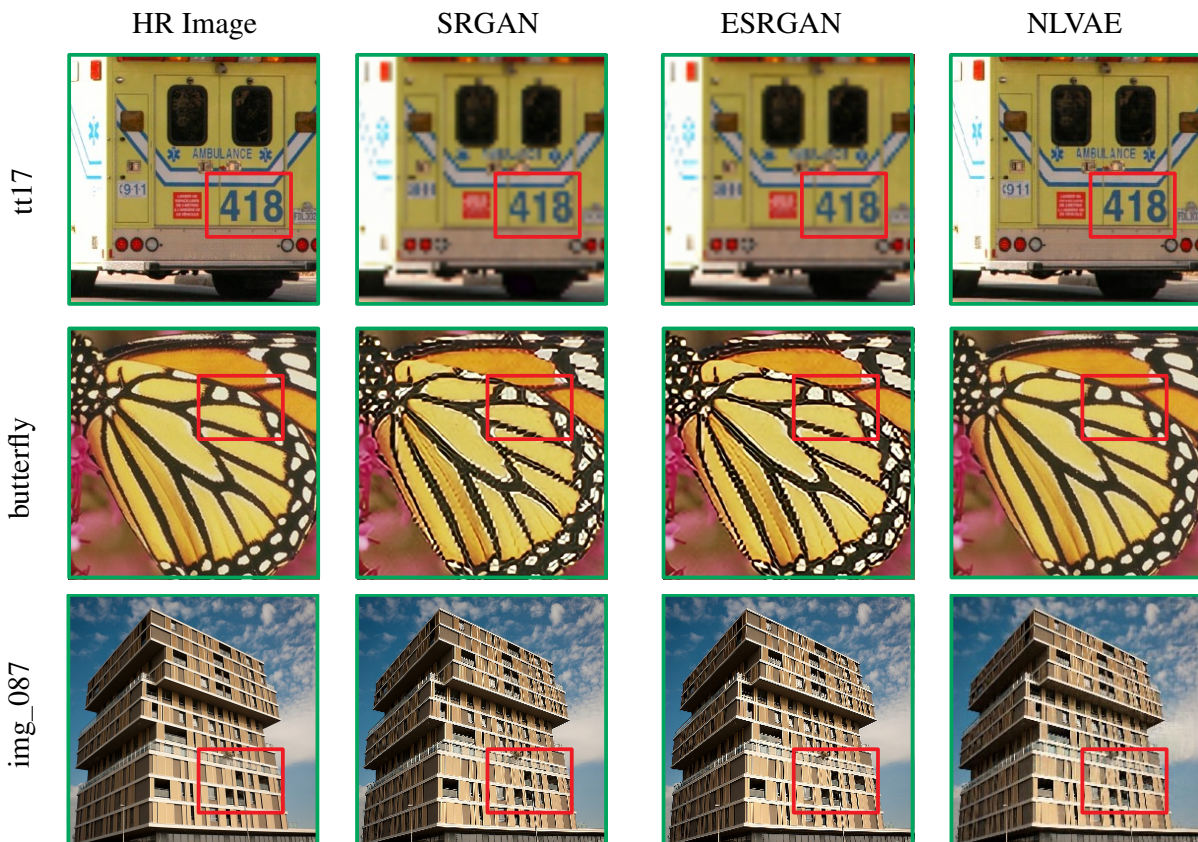


Fig. 4: Visual comparison of reconstruction-based methods on 'tt17.png' from T91 dataset and 'butterfly.png' from Set5 dataset and 'img\_087.png' Urban100

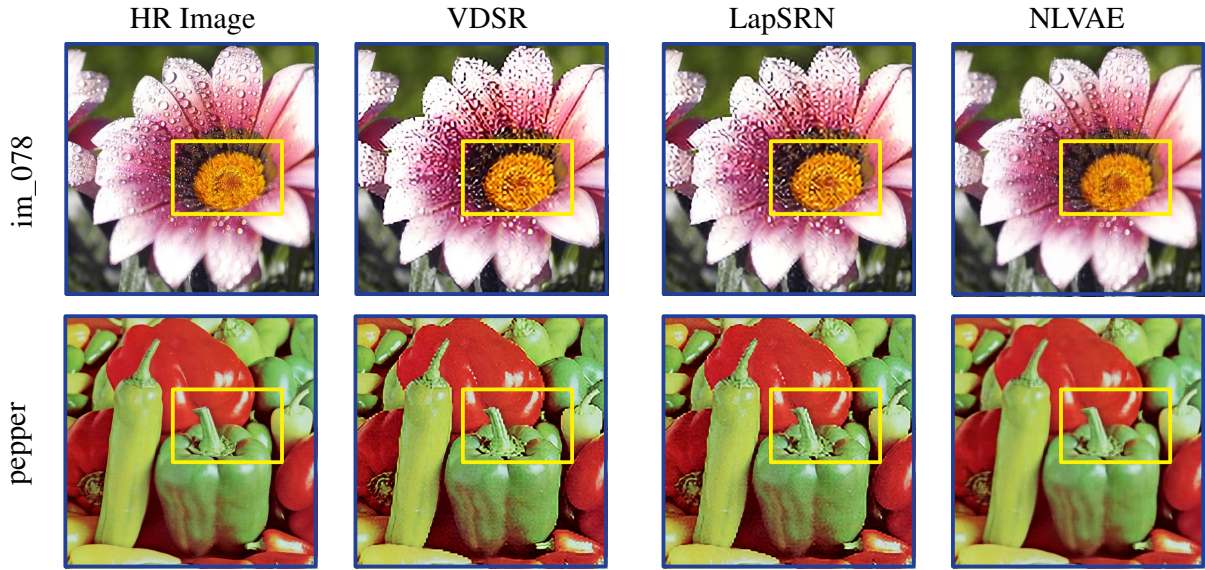
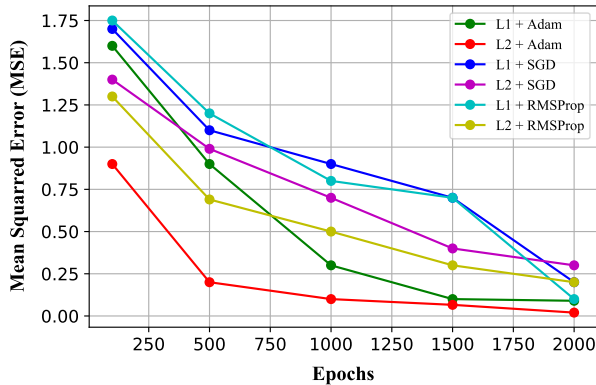
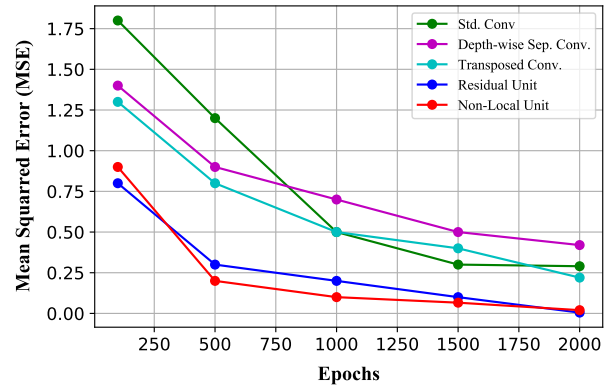


Fig. 5: Visual comparison of learning-based methods on 'im\_078.png' from General100 dataset and 'pepper.png' from Set14 dataset.



(a) L1 & L2 loss functions, and various optimizers with respect to epochs.



(b) Various feature learning units with respect to epochs.

Fig. 6: Ablation study: Evaluation of loss functions and feature learning blocks on the Set5 dataset

other reconstruction-based methods in all the scaling factors, generating high-resolution photo-realistic images. This justifies the incorporation of the non-local convolutional block which enables the model to perform better, specifically, on smaller scaled images. Moreover, the deeper architecture of the generative models enhances the performance on large scaling factors, leading the network to a robust zero-shot super-resolution network.

2) *Qualitative*: Fig. 5 and Fig. 4 depict the visualization of learning-based methods and reconstruction-based methods respectively. Samples from the Set14 and General100 datasets have been used in order to visualize the learning-based solutions. It is confirmed from Fig. 5 that our solution produces sharp edges and avoids any undesirable artifacts. As can be seen, a featured generative solution learns better representations between an LR image & its corresponding HR image. For a fair comparison with reconstruction-based solutions, we utilized Set5, Urban100, and BSDS100 for qualitative comparison among generative SISR models. The visual property of the reconstructed images is magnificent compared to

other methods because of its global contextual feature learning process. Fig. 4 demonstrates that our method can reduce the blurring artifacts presenting a powerful feature learning ability. It is imperative that the NLVAE model provides better details in regions of irregular structures. More detailed visualizations containing random HR samples from the generated sets and real datasets are provided in the supplementary material.

## V. ABLATION STUDY

### A. Loss function & Optimizers

In Fig. 6(a), we have explored different loss functions and optimizers to evaluate the performance of our proposed model. We observe that the combination  $L2 + Adam$  converges to gradient more smoothly than any other solutions. Among all optimizers, Adam converges to gradient faster than others. SGD and RMSProp provide competitive results but developing slower solutions for a zero-shot process. Between  $L2$  and  $L1$  loss functions,  $L2$  provides faster training and finer reconstruction quality. All the hyperparameters are fixed for this ablation study.

TABLE II: Number of Non-local blocks for convolutional encoder & decoder on Set5 dataset

Convolutional Encoder	PSNR	Convolutional Decoder	PSNR
Non-Local Block - 1	Unstable	Non-Local Block - 5	31.83
Non-Local Block - 2	27.45	Non-Local Block - 6	32.29
Non-Local Block - 3	30.12	Non-Local Block - 7	33.81
Non-Local Block - 4	33.27	Non-Local Block - 8	33.97
Non-Local Block - 5	34.10	Non-Local Block - 9	34.10

### B. Feature Extraction Blocks

To verify the robustness of our non-local convolutional block, we explored various feature extraction units. Fig. 6(b) shows that non-local convolutional unit performs better than other feature learning units. We observe that the residual unit learns slightly better representations than other units but has relatively larger computational burdens. Comparing our non-local unit against other traditional convolution operations (including depth-wise separable convolution, transposed convolution, and standard convolution operations) our method shows excellent performance with the lowest MSE between LR & HR images.

### C. Feature Extraction Blocks

To verify the robustness of our non-local convolutional block, we explored various feature extraction units. Fig. 6(b) shows that non-local convolutional unit performs better than other feature learning units. We observe that the residual unit learns slightly better representations than other units but has relatively larger computational burdens. Comparing our non-local unit against other traditional convolution operations (including depth-wise separable convolution, transposed convolution, and standard convolution operations) our method shows excellent performance with the lowest MSE between LR & HR images.

### D. Non-Local Blocks

In this ablations, we study the essentially of non-local blocks for image generation. In table II, the PSNR and SSIM values are depicted against number of non-local blocks for our proposed method. We note that an increase in non-local blocks provide more accurate image but also increases computational resources. Moreover, we note unusual instability using 5 or more non-local blocks with *ADAM* optimizer.

## VI. DISCUSSIONS

In this subsection, we discuss the similarity, dissimilarities and limitations of our method compared to other data-driven strategies. Table III shows that the input image is linearly upsampled before processing for super-resolution. Similar to VDSR and DRCN, we also upscale the low-resolution image but linearly. The reconstruction process in our method is progressive as we combine both learning-based and reconstruction-based methods. Learning-based methods generally utilized direct reconstruction of HR images. We

adopt the  $L_2$  loss function for faster convergence in order to maintain high-reconstruction quality. As mentioned above, we do not use a residual representation learning process due to the computational cost for self-supervised settings. Our settings use small modifications of self-supervised settings. We do not use batches of images per epochs; instead we utilize fake batches of a single image for every epochs. Moreover, we perform all these experiments on different sizes of dataset to explore structural variation. Experiments have done on small datasets (Set5, Set14) as well as large datasets (Manga109, Urban100, BSD100) to justify the performance of our proposed solution.

TABLE III: A comparison among various SISR methods defining the loss function, input types, reconstruction types and feature extraction modules.

Methods	Residual Features	Input Types	Reconstruction Types	Loss Function
SRCNN	No	LR	Direct	L2
FSRCNN	No	LR	Direct	L2
VDSR	Yes	LR + Bicubic	Direct	L2
DRCN	Yes	LR + Bicubic	Direct	L2
LapSRN	Yes	LR	Progressive	L1
NLVAE	No	LR + Linear	Progressive	L2

## VII. CONCLUSIONS

We have presented NLVAE, an untrained generative model, featuring a neural encoder-decoder framework capable of reconstructing high-resolution images. With the use of non-local convolutional modules, the model is enabled to capture high-quality semantic information. In addition, the beta variational autoencoder provides more disentangled information reconstructing high-resolution images. Combining the learning-based and reconstruction-based methods, the present method generates sharp and photo-realistic images. The effectiveness of the present model has been confirmed through an extensive experimentation compared with a number of SOTA methods, both qualitatively and quantitatively on multiple benchmark datasets. Moreover, leveraging the power of robust feature learning and generative modeling, the proposed model obviates the need for a large scale dataset while performing SISR. It is to be noted that our proposed method relies on linear upsampling before the super-resolution task. Our future work will include further validation of the NLVAE model against more challenging data settings across various domains as well as more powerful automatic upsampling strategy. We envision more extensive comprehension of our model and more intuitive design of the objective function .

## REFERENCES

- [1] R. Dian, L. Fang, and S. Li, "Hyperspectral image super-resolution via non-local sparse tensor factorization," in *Proceedings of the IEEE Conference on Computer Vision and Pattern Recognition*, 2017, pp. 5344–5353.
- [2] H.-c. Liu, S.-t. Li, and H.-t. Yin, "Infrared surveillance image super resolution via group sparse representation," *Optics Communications*, vol. 289, pp. 45–52, 2013.



- [3] Z. Wang, J. Chen, and S. C. Hoi, "Deep learning for image super-resolution: A survey," *IEEE transactions on pattern analysis and machine intelligence*, 2020.
- [4] C. Lanaras, E. Baltasavias, and K. Schindler, "Hyperspectral super-resolution by coupled spectral unmixing," in *Proceedings of the IEEE international conference on computer vision*, 2015, pp. 3586–3594.
- [5] P. Shamsolmoali, M. Zareapoor, D. K. Jain, V. K. Jain, and J. Yang, "Deep convolution network for surveillance records super-resolution," *Multimedia Tools and Applications*, vol. 78, no. 17, pp. 23 815–23 829, 2019.
- [6] D. Mahapatra, B. Bozorgtabar, and R. Garnavi, "Image super-resolution using progressive generative adversarial networks for medical image analysis," *Computerized Medical Imaging and Graphics*, vol. 71, pp. 30–39, 2019.
- [7] K.-W. Hung and W.-C. Siu, "Robust soft-decision interpolation using weighted least squares," *IEEE Transactions on Image Processing*, vol. 21, no. 3, pp. 1061–1069, 2011.
- [8] L. He, H. Qi, and R. Zaretzki, "Beta process joint dictionary learning for coupled feature spaces with application to single image super-resolution," in *Proceedings of the IEEE conference on computer vision and pattern recognition*, 2013, pp. 345–352.
- [9] K. Zeng, J. Yu, R. Wang, C. Li, and D. Tao, "Coupled deep autoencoder for single image super-resolution," *IEEE transactions on cybernetics*, vol. 47, no. 1, pp. 27–37, 2015.
- [10] J. Yang, Z. Lin, and S. Cohen, "Fast image super-resolution based on in-place example regression," in *Proceedings of the IEEE conference on computer vision and pattern recognition*, 2013, pp. 1059–1066.
- [11] J. Sun, J. Zhu, and M. F. Tappen, "Context-constrained hallucination for image super-resolution," in *2010 IEEE Computer Society Conference on Computer Vision and Pattern Recognition*. IEEE, 2010, pp. 231–238.
- [12] L. Wang, H. Wu, and C. Pan, "Fast image upsampling via the displacement field," *IEEE Transactions on Image Processing*, vol. 23, no. 12, pp. 5123–5135, 2014.
- [13] R. Fattal, "Image upsampling via imposed edge statistics," in *ACM SIGGRAPH 2007 papers*, 2007, pp. 95–es.
- [14] H. Chang, D.-Y. Yeung, and Y. Xiong, "Super-resolution through neighbor embedding," in *Proceedings of the 2004 IEEE Computer Society Conference on Computer Vision and Pattern Recognition, 2004. CVPR 2004.*, vol. 1. IEEE, 2004, pp. I–I.
- [15] K. I. Kim and Y. Kwon, "Single-image super-resolution using sparse regression and natural image prior," *IEEE transactions on pattern analysis and machine intelligence*, vol. 32, no. 6, pp. 1127–1133, 2010.
- [16] W. Ruangsang and S. Aramvith, "Efficient super-resolution algorithm using overlapping bicubic interpolation," in *2017 IEEE 6th Global Conference on Consumer Electronics (GCCE)*. IEEE, 2017, pp. 1–2.
- [17] L. Wang, S. Xiang, G. Meng, H. Wu, and C. Pan, "Edge-directed single-image super-resolution via adaptive gradient magnitude self-interpolation," *IEEE Transactions on Circuits and Systems for Video Technology*, vol. 23, no. 8, pp. 1289–1299, 2013.
- [18] M. Lu, L. Huang, and Y. Xia, "Two dimensional autoregressive modeling-based interpolation algorithms for image super-resolution: A comparison study," in *2017 10th International Congress on Image and Signal Processing, BioMedical Engineering and Informatics (CISP-BMEI)*. IEEE, 2017, pp. 1–6.
- [19] A. Shukla, S. Merugu, and K. Jain, "A technical review on image super-resolution techniques," *Advances in Cybernetics, Cognition, and Machine Learning for Communication Technologies*, pp. 543–565, 2020.
- [20] W. T. Freeman, T. R. Jones, and E. C. Pasztor, "Example-based super-resolution," *IEEE Computer graphics and Applications*, vol. 22, no. 2, pp. 56–65, 2002.
- [21] K. Zhang, X. Gao, X. Li, and D. Tao, "Partially supervised neighbor embedding for example-based image super-resolution," *IEEE Journal of Selected Topics in Signal Processing*, vol. 5, no. 2, pp. 230–239, 2010.
- [22] J. Kim, J. Kwon Lee, and K. Mu Lee, "Accurate image super-resolution using very deep convolutional networks," in *Proceedings of the IEEE conference on computer vision and pattern recognition*, 2016, pp. 1646–1654.
- [23] H. Gupta, K. H. Jin, H. Q. Nguyen, M. T. McCann, and M. Unser, "Cnn-based projected gradient descent for consistent ct image reconstruction," *IEEE transactions on medical imaging*, vol. 37, no. 6, pp. 1440–1453, 2018.
- [24] K. Zhang, X. Gao, D. Tao, and X. Li, "Single image super-resolution with non-local means and steering kernel regression," *IEEE Transactions on Image Processing*, vol. 21, no. 11, pp. 4544–4556, 2012.
- [25] V. K. Ha, J. Ren, X. Xu, S. Zhao, G. Xie, and V. M. Vargas, "Deep learning based single image super-resolution: A survey," in *International Conference on Brain Inspired Cognitive Systems*. Springer, 2018, pp. 106–119.
- [26] J. Kim, J. Kwon Lee, and K. Mu Lee, "Deeply-recursive convolutional network for image super-resolution," in *Proceedings of the IEEE conference on computer vision and pattern recognition*, 2016, pp. 1637–1645.
- [27] A. Bhowmik, S. Shit, and C. S. Seelamantula, "Training-free, single-image super-resolution using a dynamic convolutional network," *IEEE signal processing letters*, vol. 25, no. 1, pp. 85–89, 2017.
- [28] W.-S. Lai, J.-B. Huang, N. Ahuja, and M.-H. Yang, "Deep laplacian pyramid networks for fast and accurate super-resolution," in *Proceedings of the IEEE conference on computer vision and pattern recognition*, 2017, pp. 624–632.
- [29] Y. Zhang, K. Li, K. Li, B. Zhong, and Y. Fu, "Residual non-local attention networks for image restoration," in *International Conference on Learning Representations*, 2019. [Online]. Available: <https://openreview.net/forum?id=HkeGhoA5FFX>
- [30] B. Lim, S. Son, H. Kim, S. Nah, and K. Mu Lee, "Enhanced deep residual networks for single image super-resolution," in *Proceedings of the IEEE conference on computer vision and pattern recognition workshops*, 2017, pp. 136–144.
- [31] Y. Hu, J. Li, Y. Huang, and X. Gao, "Channel-wise and spatial feature modulation network for single image super-resolution," *IEEE Transactions on Circuits and Systems for Video Technology*, 2019.
- [32] X.-J. Mao, C. Shen, and Y.-B. Yang, "Image restoration using very deep convolutional encoder-decoder networks with symmetric skip connections," in *Proceedings of the 30th International Conference on Neural Information Processing Systems*, 2016, pp. 2810–2818.
- [33] Y. Tai, J. Yang, and X. Liu, "Image super-resolution via deep recursive residual network," in *Proceedings of the IEEE conference on computer vision and pattern recognition*, 2017, pp. 3147–3155.
- [34] J. S. Park, J. W. Soh, and N. I. Cho, "High dynamic range and super-resolution imaging from a single image," *IEEE Access*, vol. 6, pp. 10 966–10 978, 2018.
- [35] W. Shi, J. Caballero, F. Huszár, J. Totz, A. P. Aitken, R. Bishop, D. Rueckert, and Z. Wang, "Real-time single image and video super-resolution using an efficient sub-pixel convolutional neural network," in *Proceedings of the IEEE conference on computer vision and pattern recognition*, 2016, pp. 1874–1883.
- [36] C. Dong, C. C. Loy, and X. Tang, "Accelerating the super-resolution convolutional neural network," in *European conference on computer vision*. Springer, 2016, pp. 391–407.
- [37] Z. Hua, H. Zhang, and J. Li, "Image super resolution using fractal coding and residual network," *Complexity*, vol. 2019, 2019.
- [38] G. F. Montufar, R. Pascanu, K. Cho, and Y. Bengio, "On the number of linear regions of deep neural networks," in *Advances in neural information processing systems*, 2014, pp. 2924–2932.
- [39] S. Lian, H. Zhou, and Y. Sun, "Fg-srgan: A feature-guided super-resolution generative adversarial network for unpaired image super-resolution," in *International Symposium on Neural Networks*. Springer, 2019, pp. 151–161.
- [40] X. Dou, C. Li, Q. Shi, and M. Liu, "Super-resolution for hyperspectral remote sensing images based on the 3d attention-srgan network," *Remote Sensing*, vol. 12, no. 7, p. 1204, 2020.
- [41] S. Bell-Kligler, A. Shocher, and M. Irani, "Blind super-resolution kernel estimation using an internal-gan," in *Advances in Neural Information Processing Systems*, 2019, pp. 284–293.
- [42] T. R. Shaham, T. Dekel, and T. Michaeli, "Singan: Learning a generative model from a single natural image," in *Proceedings of the IEEE International Conference on Computer Vision*, 2019, pp. 4570–4580.
- [43] C. Ledig, L. Theis, F. Huszár, J. Caballero, A. Cunningham, A. Acosta, A. Aitken, A. Tejani, J. Totz, Z. Wang *et al.*, "Photo-realistic single image super-resolution using a generative adversarial network," in *Proceedings of the IEEE conference on computer vision and pattern recognition*, 2017, pp. 4681–4690.
- [44] X. Wang, K. Yu, S. Wu, J. Gu, Y. Liu, C. Dong, Y. Qiao, and C. Change Loy, "Esrgan: Enhanced super-resolution generative adversarial networks," in *Proceedings of the European Conference on Computer Vision (ECCV)*, 2018, pp. 0–0.
- [45] M. M. Majdabadi and S.-B. Ko, "Capsule gan for robust face super resolution," *Multimedia Tools and Applications*, vol. 79, no. 41, pp. 31 205–31 218, 2020.
- [46] J. Qiao, H. Song, K. Zhang, X. Zhang, and Q. Liu, "Image super-resolution using conditional generative adversarial network," *IET Image Processing*, vol. 13, no. 14, pp. 2673–2679, 2019.
- [47] A. Van Den Oord, N. Kalchbrenner, and K. Kavukcuoglu, "Pixel recurrent neural networks," in *Proceedings of the 33rd International*

- Conference on International Conference on Machine Learning-Volume 48*, 2016, pp. 1747–1756.
- [48] A. Van den Oord, N. Kalchbrenner, L. Espeholt, O. Vinyals, A. Graves *et al.*, “Conditional image generation with pixelcnn decoders,” *Advances in neural information processing systems*, vol. 29, pp. 4790–4798, 2016.
- [49] I. Goodfellow, “Nips 2016 tutorial: Generative adversarial networks,” *arXiv preprint arXiv:1701.00160*, 2016.
- [50] N. Takano and G. Alaghband, “Srgan: Training dataset matters,” *arXiv preprint arXiv:1903.09922*, 2019.
- [51] H. Wang, D. Su, C. Liu, L. Jin, X. Sun, and X. Peng, “Deformable non-local network for video super-resolution,” *IEEE Access*, vol. 7, pp. 177 734–177 744, 2019.
- [52] D. Liu, B. Wen, Y. Fan, C. C. Loy, and T. S. Huang, “Non-local recurrent network for image restoration,” in *Advances in Neural Information Processing Systems*, 2018, pp. 1673–1682.
- [53] Y. Mei, Y. Fan, Y. Zhou, L. Huang, T. S. Huang, and H. Shi, “Image super-resolution with cross-scale non-local attention and exhaustive self-exemplars mining,” in *Proceedings of the IEEE/CVF Conference on Computer Vision and Pattern Recognition*, 2020, pp. 5690–5699.
- [54] A. Shocher, N. Cohen, and M. Irani, ““zero-shot” super-resolution using deep internal learning,” in *Proceedings of the IEEE Conference on Computer Vision and Pattern Recognition*, 2018, pp. 3118–3126.
- [55] D. Ulyanov, A. Vedaldi, and V. Lempitsky, “Deep image prior,” in *Proceedings of the IEEE Conference on Computer Vision and Pattern Recognition*, 2018, pp. 9446–9454.
- [56] Y. Bengio, A. Courville, and P. Vincent, “Representation learning: A review and new perspectives,” *IEEE transactions on pattern analysis and machine intelligence*, vol. 35, no. 8, pp. 1798–1828, 2013.
- [57] S. Ioffe and C. Szegedy, “Batch normalization: Accelerating deep network training by reducing internal covariate shift,” *arXiv preprint arXiv:1502.03167*, 2015.
- [58] D. P. Kingma and M. Welling, “Auto-encoding variational bayes,” *arXiv preprint arXiv:1312.6114*, 2013.
- [59] J.-L. Durrieu, J.-P. Thiran, and F. Kelly, “Lower and upper bounds for approximation of the kullback-leibler divergence between gaussian mixture models,” in *2012 IEEE International Conference on Acoustics, Speech and Signal Processing (ICASSP)*. Ieee, 2012, pp. 4833–4836.
- [60] R. T. Chen, X. Li, R. B. Grosse, and D. K. Duvenaud, “Isolating sources of disentanglement in variational autoencoders,” in *Advances in Neural Information Processing Systems*, 2018, pp. 2610–2620.
- [61] E. Mathieu, T. Rainforth, N. Siddharth, and Y. W. Teh, “Disentangling disentanglement in variational autoencoders,” in *International Conference on Machine Learning*, 2019, pp. 4402–4412.
- [62] I. Higgins, L. Matthey, A. Pal, C. Burgess, X. Glorot, M. Botvinick, S. Mohamed, and A. Lerchner, “beta-vae: Learning basic visual concepts with a constrained variational framework,” 2016.
- [63] R. Timofte, V. De Smet, and L. Van Gool, “A+: Adjusted anchored neighborhood regression for fast super-resolution,” in *Asian conference on computer vision*. Springer, 2014, pp. 111–126.
- [64] C. Dong, C. C. Loy, K. He, and X. Tang, “Image super-resolution using deep convolutional networks,” *IEEE transactions on pattern analysis and machine intelligence*, vol. 38, no. 2, pp. 295–307, 2015.
- [65] Y. Tai, J. Yang, X. Liu, and C. Xu, “Memnet: A persistent memory network for image restoration,” in *Proceedings of the IEEE international conference on computer vision*, 2017, pp. 4539–4547.
- [66] M. Bevilacqua, A. Roumy, C. Guillemot, and M. L. Alberi-Morel, “Low-complexity single-image super-resolution based on nonnegative neighbor embedding,” 2012.
- [67] R. Zeyde, M. Elad, and M. Protter, “On single image scale-up using sparse-representations,” in *International conference on curves and surfaces*. Springer, 2010, pp. 711–730.
- [68] D. Martin, C. Fowlkes, D. Tal, and J. Malik, “A database of human segmented natural images and its application to evaluating segmentation algorithms and measuring ecological statistics,” in *Proceedings Eighth IEEE International Conference on Computer Vision. ICCV 2001*, vol. 2. IEEE, 2001, pp. 416–423.
- [69] Y. Matsui, K. Ito, Y. Aramaki, A. Fujimoto, T. Ogawa, T. Yamasaki, and K. Aizawa, “Sketch-based manga retrieval using manga109 dataset,” *Multimedia Tools and Applications*, vol. 76, no. 20, pp. 21 811–21 838, 2017.
- [70] J.-B. Huang, A. Singh, and N. Ahuja, “Single image super-resolution from transformed self-exemplars,” in *Proceedings of the IEEE conference on computer vision and pattern recognition*, 2015, pp. 5197–5206.
- [71] J. Yang, J. Wright, T. S. Huang, and Y. Ma, “Image super-resolution via sparse representation,” *IEEE transactions on image processing*, vol. 19, no. 11, pp. 2861–2873, 2010.
- [72] D. P. Kingma and J. Ba, “Adam: A method for stochastic optimization,” *arXiv preprint arXiv:1412.6980*, 2014.